Article

Not peer-reviewed version

Study of the Structure and Mechanical Properties of Ti-38Zr-11Nb Alloy

Konstantin V. Sergienko *, Sergei V. Konushkin, Yaroslava A. Morozova, Mikhail A. Kaplan, Artem D. Gorbenko, Boris A. Rumyantsev, Mikhail E. Prutskov, Evgeny E. Baranov, Elena O. Nasakina, Tatiana M. Sevostyanova, Sofia A. Mikhlik, Andrey P. Chizhikov, Lyudmila A. Shatova, Aleksandr V. Simakin, Ilya V. Baimler, Maria A. Sudarchikova, Mikhail L. Kheifetz, Alexey G. Kolmakov, Mikhail A. Sevostyanov

Posted Date: 24 February 2025

doi: 10.20944/preprints202502.1884.v1

Keywords: titanium alloys; zirconium alloys; Young's modulus; mechanical properties; implants; medical materials

Article

Study of the Structure and Mechanical Properties of Ti-38Zr-11Nb Alloy

Konstantin V. Sergienko [1,*], Sergei V. Konushkin [1], Yaroslava A. Morozova [1], Mikhail A. Kaplan [1], Artem D. Gorbenko [1], Boris A. Rumyantsev [1],Mikhail E. Prutskov [1], Evgeny E. Baranov [1], Elena O. Nasakina [1], Tatiana M. Sevostyanova [2,3], Sofia A. Mikhlik [1], Andrey P. Chizhikov [4], Lyudmila A. Shatova [5], Aleksandr V. Simakin [6], Ilya V. Baimler [6], Maria A. Sudarchikova [1], Mikhail L. Kheifetz [7], Alexey G. Kolmakov [1] and Mikhail A. Sevostyanov [1,8]

[1] A.A. Baikov Institute of Metallurgy and Materials Science, Russian Academy of Sciences (IMET RAS), 119334 Moscow, Russia
[2] National Medical and Surgical Center Named after N.I. Pirogov of the Ministry of Health of the Russian Federation, 117513 Moscow, Russia
[3] Moscow Regional Research and Clinical Institute ("MONIKI"), 129110 Moscow, Russia
[4] Institute of Structural Macrokinetics and Materials Science, Russian Academy of Sciences (ISMAN), 142432 Chernogolovka, Russia
[5] Voronezh State Technical University, Faculty of Radio Engineering and Electronics, 394026 Voronezh, Russia
[6] Prokhorov General Physics Institute of the Russian Academy of Sciences, Vavilov Str. 38, 119991 Moscow, Russia
[7] Institute of Applied Physics, NAS of Belarus, Minsk, Belarus
[8] All-Russia Scientific Research Institute of a Phytopathology (VNIIF), 143050 Bolshye Vyazemy settlement, Moscow region, Russia
* Correspondence: shulf@yandex.ru; Tel.: +7-9581998137

Abstract: Hip joint implants are one of the most common types of medical implants used to replace a damaged joint and restore its functional activity. Hundreds of thousands of surgeries are performed annually to install them, which underscores the importance of developing and improving materials for such implants. Modern materials for implants, including cobalt-chromium alloys, stainless steel, titanium and other titanium alloys, face problems such as the toxicity of certain elements (for example, aluminum, vanadium, nickel) and excessive Young's modulus, which negatively affects biomechanical compatibility. A mismatch between the stiffness of the implant material and the bone tissue, called stress shielding, can lead to bone resorption and loosening of the implant. Recent studies have shifted the focus to β-titanium alloys due to their exceptional biocompatibility, corrosion resistance, and low Young's modulus, which is close to the Young's modulus of bone tissue (10-30 GPa). Among them, Ti-38Zr-11Nb alloy is promising for use as an implant material. In this study, the microstructure, mechanical properties, and phase stability of Ti-38Zr-11Nb alloy were studied. Energy dispersion spectrometry confirmed the homogeneous distribution of Ti, Zr, and Nb in the alloy. Microstructural analysis revealed elongated β-grains after rolling and quenching, and grinding contributed to recrystallization and the formation of subgrains. X-ray diffraction analysis confirmed the presence of a stable β-phase under any heat treatment conditions, which is explained by the use of Nb as a β-stabilizer and Zr as a neutral element with a weak β-stabilizing effect in the presence of other β-stabilizers. The modulus of elasticity after annealing decreased from 85 GPa to 81 GPa. Mechanical tests showed a significant increase in tensile strength (from 529 MPa to 628 MPa) simultaneously with a 32% decrease in elongation to fracture of the samples. These changes are caused by microstructural transformations such as the formation of subgrains and rearrangement of dislocations. Based on the results of the study, it can be concluded that Ti-38Zr-11Nb alloy is a promising material due to its lower low Young's modulus relative to the classical materials used and stable β-phase, which provides the possibility of long-term use of the implant, without the risk of formation of brittle phases.

Keywords: titanium alloys; zirconium alloys; Young's modulus; mechanical properties; implants; medical materials

 doi:10.20944/preprints202502.1884.v1

1. Introduction

The hip joint is one of the most stressed elements of the human musculoskeletal system [1] In the presence of the development of degenerative joint diseases or serious joint damage as a result of injuries, implantation of an artificial hip joint may be recommended to replace the lost healthy one. For the manufacture of the leg and cup of the hip joint, it is necessary to use materials that provide a set of properties: biocompatibility, sufficient mechanical properties, corrosion resistance, and the value of the Young's modulus close to the value of the bone index. There is an annual increase in the number of such operations, which is associated with a number of factors, such as an increase in the life span of the population, increased availability of such operations in different parts of the world, increased awareness of the possible prospects for the use of artificial joints and an increased relative number of successful operations [2,3]. The materials used in hip arthroplasty today belong to the following material groups: cobalt-chromium alloys, stainless steel, titanium and titanium alloys. [4–6]

Despite their high strength and corrosion resistance, some of these materials contain elements that are toxic to the human body, such as aluminum, vanadium and nickel [7–10], and their elastic modulus (Young's modulus) is much higher than that of bone tissue [11,12], which can negatively affect biomechanical compatibility due to the risk of aseptic loosening, wear, and mismatch of the mechanical properties of the implant with those of the bone tissue [13].

The modulus of elasticity (E) is a key mechanical property of a material that determines its stiffness and ability to resist deformation in tension or compression . For materials used in endoprosthetics, it is critical that the modulus of elasticity be as close as possible to that of bone tissue, which is in the range of 10-30 GPa [14,15]. This match ensures optimal mechanical biocompatibility between the implant and the surrounding bone tissue, which promotes uniform load distribution and minimizes the risk of localized overstress in the bone-implant system [16–20].

When the Young's modulus of the implant material is significantly higher than that of the bone, a phenomenon known as stress shielding occurs. In this case, the load is distributed unevenly between the implant leg and the bone into which it is integrated. Thus, there is an atypically low local load on a part of the bone tissue, as a result of which the rate of bone resorption begins to exceed the rate of bone formation. For example, cobalt-chromium alloys, which have high strength and wear resistance, have high stiffness (Young's modulus ~134-230 GPa) [21,22]. Stainless steel is less commonly used due to its lower biocompatibility and corrosion resistance, and its Young's modulus is high at ~190-210 GPa, [23,24] which also exceeds the Young's modulus of bone tissue (10-30 GPa). Titanium and titanium alloys are widely used because of their excellent biocompatibility, corrosion resistance, and moderate Young's modulus (~100-110 GPa for Ti-6Al-4V), but pure titanium and most of its alloys (with α, α+β phase) still have an excessive Young's modulus relative to bone tissue, which can lead to uneven load distribution. According to Wolff's Law, bone adapts to the applied loads: insufficient mechanical stimulation activates bone resorption processes, leading to gradual thinning and weakening of the bone. This leads to a violation of the fixation of the implant and further loosening of the implant, which necessitates a second operation to replace the implant leg.

In connection with the above, the study of materials with a lower Young's modulus relative to the materials used can reduce the effect of bone destruction over time and lead to a longer period of operation of the product.

For a long time, β titanium alloys were not of interest to industry, but recent research and a new look at the applicability of materials find in them a promising replacement for the materials currently used due to a successful combination of properties such as high biocompatibility, decent corrosion resistance and, most importantly, a lower Young's modulus relative to Ti–6Al-4V and cobalt- chrome alloys. The development of β–titanium alloys with a Young's modulus of about 50-80 GPa makes it possible to create bone implants with a more natural stiffness, and as a result, minimizing the risk of

 doi:10.20944/preprints202502.1884.v1

stress shielding with further bone resorption. In addition, the optimization of the phase composition (predominance of β-phase) and the alloying with biocompatible elements (e.g. Zr, Nb) allow the elimination of toxic components and improve osseointegration. . [1–5] These advantages pave the way for the development of durable implants capable of providing uniform load distribution and reducing the frequency of revision surgery. However, to introduce such alloys into clinical practice, further research is needed to optimize their composition, assess their fatigue resistance and longterm stability in biological environments. This work contributes to these challenges by focusing on analyzing the relationship between structure, phase composition and mechanical properties of β-titanium alloys, which is a critical step towards their practical application in endoprosthetics.

The purpose of this study is to develop and comprehensively evaluate a titanium alloy containing zirconium and niobium for use as a material for bone implants. The aim of this work was to analyze the stability of the phase composition after annealing and on the mechanical, cyclic and superelastic properties of the alloy. We paid extra care to look at Young's modulus, which is a main factor in how well the mix works with human bone. This is key for making the implants last longer and work better. In this work, we checked both the physical and strength features of the mix.

2. Materials and Methods

2.1. Selection of the Object of Research

In this work has been studied (at.%): Ti-38Zr-11Nb. Titanium produced by VSMPO-AVISMA Corporation (Russia), zirconium and niobium produced by Chepetskiy Mechanical Plant (Russia) were used. The Mo equivalent is an empirical parameter representing the contribution of the alloying elements to the stability of the β-phase relative to Mo [6].

To perform the calculation, it is necessary to convert atomic percentages to mass percentages (Table 1):

Table 1. Conversion of atomic percentage to mass percentage.

Chemical Element	Atomic Mass (a.e.m.)	Atomic Percentage (%)	Atomic Mass * Atomic Percent =	Mass Percentage (%)
Ti	47.87	50	2393.5	34
Nb	92.91	11	1022.01	15
Zr	91.22	39	3557.58	51

Taking into account the mass percentages and literature data on the contribution of the alloying elements, we make a calculation:

[Mo] eq = 0.28 * [%mass Nb] + 0.08 * [%mass Zr]

When estimating the molybdenum equivalent of a complex alloy, the effect of different β-stabilizers is considered additive and the influence of α-stabilizers and neutral hardeners is neglected. Thus the effect of Nb on β-phase stability is 1/3.6=0.28, i.e., niobium is 3.6 times weaker in stabilizing the beta-phase and zirconium is 14 times weaker than molybdenum, the effect of Zr on β-phase stability is 1/14=0.08. [6,7]

Calculation of the molybdenum equivalent:

[Mo] eq = %Nb*0.28 + %Zr*0.08 = 15*0.28 + 51*0.08= 8.28

From the data obtained and the information in Table 2, it can be concluded that the alloy studied have an α+β phase in the annealed state; therefore, by means of thermomechanical treatment, namely plastic deformation and quenching, alloys with an unstable β phase, low Young's modulus and superelasticity effect can be obtained from them.

Table 2. Value of molybdenum equivalent as a function of alloy phase composition [Adapted from Ref. [7]].

Alloy Grade	[Mo] Equivalent
(α + β)-alloys	3.3–10

 doi:10.20944/preprints202502.1884.v1

Pseudo β-alloys	11.0–16.3
β-alloys	16.9

2.2. Production and Processing of Research Samples

The alloy samples were melted in a copper water-cooled crystallizer in an argon arc furnace with a non-expendable tungsten electrode L200DI (Leybold-Heraeus, Hanau, Germany) at an argon pressure of 40×10^3 Pa. The following were used as charge materials: titanium (Ti-1 grade), zirconium (Zr-1 grade), and niobium (Hb-1 grade). The materials were placed in a copper water-cooled tray of a vacuum electric arc furnace as follows: titanium was placed at the bottom of the crystallizer wells, then zirconium, and niobium on top. The order of arrangement of initial metals corresponded to the melting temperature of each material, and melting was carried out by arc directed from top to bottom. In addition, zirconium was placed in a separate pan to act as a getter. The furnace was vacuumed to a residual pressure of 1.33 Pa and filled with high purity inert argon gas. First, the zirconium getter is melted after induction into the inert gas chamber to remove possible oxygen impurities in the gas. Next, the starting materials are melted until individual ingots are formed. Remelting was carried out 7 times, with the ingots being turned over for better mixing of the raw materials. The specified number of remelting operations helped to achieve uniformity of chemical composition throughout the ingot volume. The duration of each ingot melting was 1-1.5 min. After melting, the ingot had the shape of a "boat" with length ~120 mm, width ~25 mm, height ~12 mm.

The obtained ingots have a dendritic structure. Homogenizing annealing in a vacuum resistance furnace ESKVE-1.7.2.5/21 ShM13 (NITTIN, Moscow, Russia) at 1000 °C for 4 h was used to homogenize the structure and remove stresses. To protect against oxidation, annealing was performed in a vacuum environment at 27×10^{-4} Pa

Primary deformation of ~18 mm thick castings was carried out by warm rolling at preheating to a temperature of 700 °C on a double-roller mill, DUO-300 (AO Istok ML, Fryazino, Moscow Oblast, Russia), with partial absolute compressions per pass: 1.5 mm down to billet thickness of 4.0 mm (heating every 2 passes, total 10 passes), then 1.0 mm down to billet thickness of 2.0 mm (heating every pass, total 2 passes), and a further 0.5 mm down to final billet thickness—1 mm (heating before the first pass at thickness of 2 mm, total 2 passes). The billets were heated before deformation in a muffle furnace KYLS 20.18.40/10 (Hans Beimler, Leipzig, Germany) to a temperature of 600°C for 20 min before the first rolling and for 5 min during intermediate annealing. The plates were cold-rolled from a thickness of 1.5 mm. The effect of heat treatment on the structure and mechanical properties of Ti-38Zr-11Nb alloys was investigated on samples cut from plates with a final thickness of 1 mm using a DK7745 Electrical discharge machining (Meatec, Moscow, Russia). Prior to this, the plate (length ~640 mm, width ~56 mm, height ~1 mm) was quenched by heating for 5 min at 600°C and cooling in room temperature water. During the rolling and quenching process, a thin oxide layer was formed on the plate surface. This layer was removed by mechanical grinding.

Preparation of samples for metallographic study was carried out by sequential grinding on a Phoenix 4000 machine (Buehler, Lake Bluff, Illinois, USA). The microstructure was revealed and analyzed by etching in a weak solution of hydrofluoric and nitric acids with distilled water in the ratio of 10% HF: 10% HNO3: 80% H2O for 20–30 s. After, the microstructure was rinsed with distilled water, and residual water was removed by air flow.

2.3. Methods of Research

To determine oxygen and nitrogen impurities, we used reducing melting in a graphite crucible in a helium-fueled pulse resistance furnace using the TC-600 analyzer (LECO, 3000 Lakeview Avenue, St.Joseph, MI 49085-2396, USA). Nitrogen was detected by thermal conductivity, and oxygen was detected by the amount of released CO2 using the infrared absorption method.

To determine hydrogen impurities, we used reducing melting in a graphite crucible in an argon-fueled pulse resistance furnace using the RHEN-602 analyzer (LECO, 3000 Lakeview Avenue, St.Joseph, MI 49085-2396, USA). Hydrogen was detected by thermal conductivity.

 doi:10.20944/preprints202502.1884.v1

To determine carbon and sulfur impurities, we used oxidizing melting in a ceramic crucible in an induction furnace with the flux using a CS-600 analyzer (LECO, 3000 Lakeview Avenue, St.Joseph, MI 49085-2396, USA). The elements were detected by the amount of released CO2 and SO2 using the infrared absorption method. The distribution of elements was studied using the scanning electron microscope (SEM) EM6900 (KYKY, Beijing, China) with an EDS detector from Oxford Instruments (Oxford Instruments, Abingdon, Oxfordshire, United Kingdom) using Aztec software.

X-ray phase analysis was performed on the DX2700mini diffractometer (Dandong Haoyuan Instrument Co., Dandong City, Liaoning Province, China). The studies were carried out in CuKα = 1.54178 Å radiation, 2θ = 20-100° range, the shooting step was 0.02°/s, the holding time per step was 0.2 s, the voltage on the tube was 40 kV, the current was 13 mA. The analysis of the obtained diffraction patterns was carried out in the Match! 3 program.

For optical examination of the microstructure, the samples were pre-pressed in a rigid mold into cylinders by means of one-sided pressing.

The samples were pressed on an IPA 40 air-hydraulic press (Remet, Bologna, Italy) into Aka-Resin Epoxy resin at temperatures of 160…185°C and a holding time of 20 minutes. The sample was placed in a mold, filled with granulated resin, after which the chamber was closed and the sample was pressed to a pressure of 6 bar. The device then performed a given program, after which the pressed sample was ground and polished. Polishing and grinding of samples for examination on an optical microscope were carried out in the following sequence.

• On a Piatto diamond disc with the following grit:

P220 for 10 min
P600 for 10 min
P1000 for 5 min
P1200 for 5 min
P2500 for 5 min
P4000 for 5 min

• On an Akasel NAPAL velvet polishing wheel with a DiaMaxx Poly diamond suspension with particle sizes of 1 μm and 50 nm for 5 min for each suspension.

A Phoenix 4000 polishing machine(Buehler, Lake Bluff, Illinois, USA) was used for grinding and polishing.

The surface of the samples was etched with a solution of nitric and hydrofluoric acids with distilled water in a ratio of HF: HNO3: 15 H2O by volume. The sections were immersed in the etching solution for 5–30 s, then washed with running water.

Light microscopy was carried out on the MET 5C (Altami, Saint Petersburg, Russia) microscope using a high-resolution video camera built into the device and Altami Studio 4.0 software. [8]

Nanohardness and Young's modulus were determined using a NanoScan-4D nanohardness tester (NauchSpecPribor, Troitsk, Russia). Instrumental indentation was performed according to ISO 14577-1:2002 [9]. All specimens were subjected to instrumental indentation into the matrix with a load of 500 mN using a Berkovich type diamond tip. Measurements were taken across the full width of the specimen. The load/unload rate was 20 mN/s, the contact time was 20 s, and the distance between indentations was 200 μm. The number of indentations for each treatment type was 27. The experimental curves were processed using NANOINDENTATION 3.0 software from CSM Instruments (Switzerland) with a specified Poisson's ratio (0.3) and averaged over five experimental curves. Elastic recovery was defined as the ratio of elasticity to total indentation work. Fractographic studies were carried out on a KYKY EM6900 (KYKY, Beijing, China) scanning electron microscope using a secondary electron detector at an accelerating voltage of 20 kV.

Static mechanical tests were performed on an INSTRON 3382 universal testing machine (Instron, Norwood, MA, USA) at a tensile speed of 1 mm/min using flat specimens of 28 × 6 × 1 mm and a working part size of 15 × 3 × 1 mm. The number of specimens for each alloy and treatment type was 9. The processing of the test results to determine the characteristics of mechanical properties was carried out in accordance with GOST 1497-84 using INSTRON Bluehill 2.0 software. The following

 doi:10.20944/preprints202502.1884.v1

parameters were determined: conditional yield strength $\sigma_{0.2}$, tensile strength σ_v and relative elongation δ.

Cyclic tests to determine the hysteresis behavior of the material were performed on an INSTRON 3382 universal testing machine. For each specimen, 10 cycles were performed; in the first part of the cycle, the specimen was stretched at a rate of 1 mm/min until the working area was elongated by 8%, and in the second part of the cycle, the specimen was compressed at a rate of 1 mm/min to the original size. The best hysteresis behavior can be used to evaluate the superplasticity effect of the alloys studied. Strain measurement was performed with an additional probe mounted directly on the specimen with two clamps along the edge of the specimen work area, so that the tensile value of the specimen work area was more accurate and did not include the strain of the gripping parts of the specimen, which occurs when using tensile values from the INSTRON 3382 frame-mounted probe. The specimen dimensions were 56 × 10 × 1 mm and the workspace size was 32 × 6 × 1 mm.

3. Results

3.1. Chemical Analysis of Alloy Plates by Energy-Dispersive Spectrometry

The results of chemical analysis of Ti-38Zr-11Nb alloy plates by energy-dispersive spectrometry show the uniformity of element distribution over the studied area, as well as the result at selected points on the plate surface. The electron image of the studied area and the uniformity of chemical element distribution, as well as the points of composition analysis are shown in the images in Figure 1 (a-d).

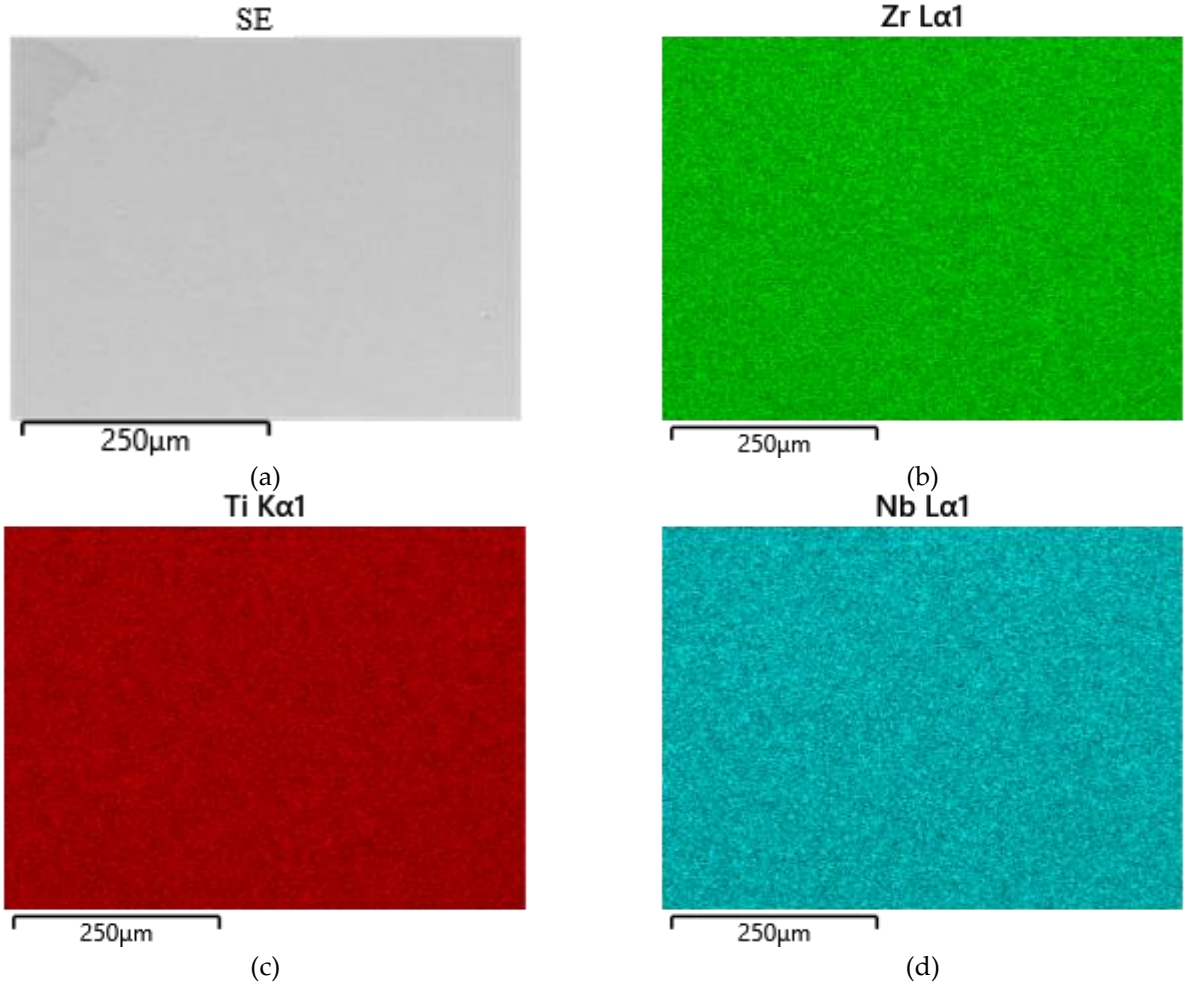

Figure 1. Distribution of elemental composition by area.

Confirmed alloy composition: Ti - 51.8% (at.), Zr - 37.1% (at.), Nb - 11.1% (at.). An example of the spectrum obtained for three points is shown in Figure 2.

Preprints.org (www.preprints.org) | NOT PEER-REVIEWED | Posted: 24 February 2025 doi:10.20944/preprints202502.1884.v1

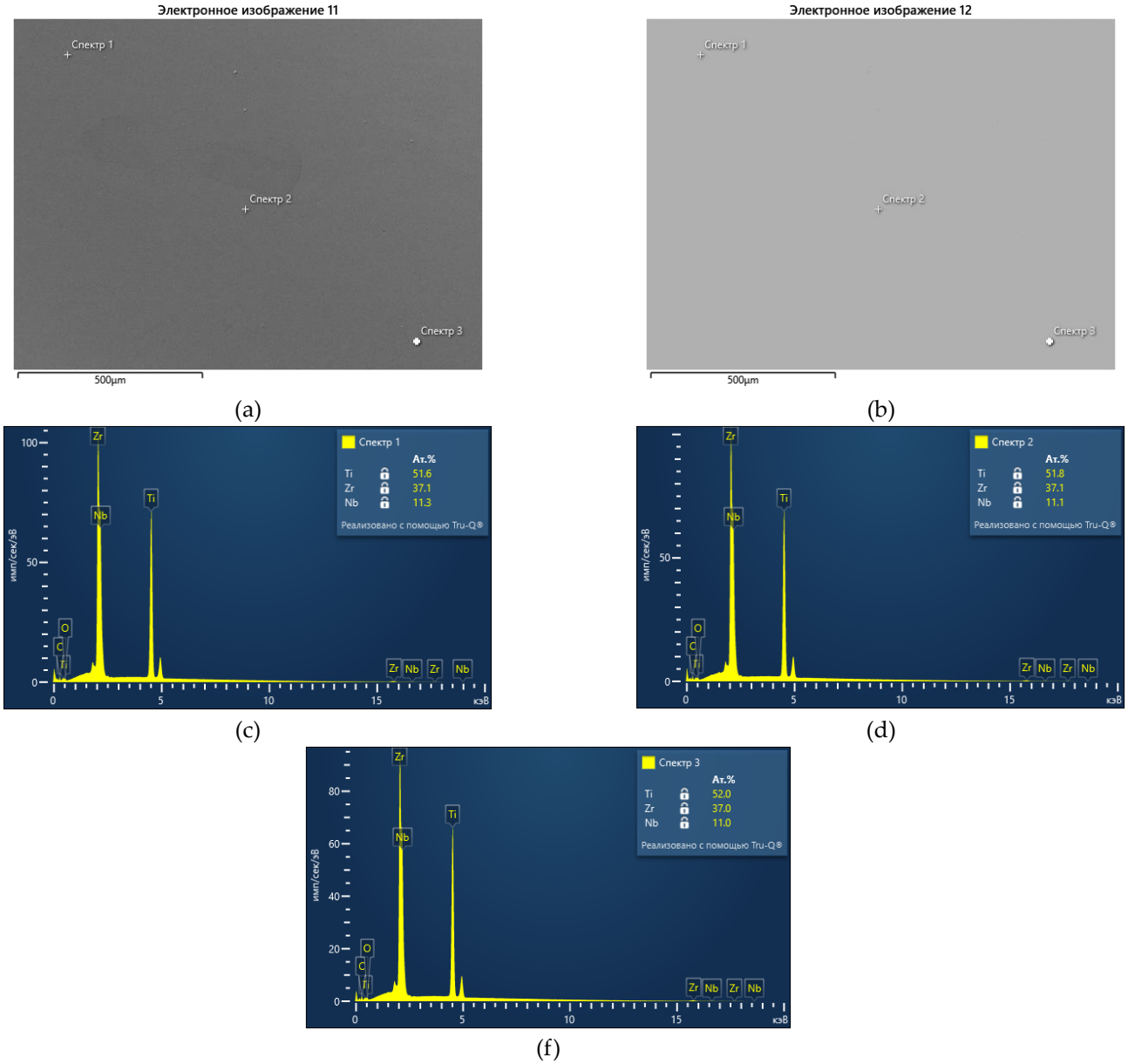

Figure 2. Results of chemical analysis of polished Ti-38Zr-11Nb alloy plate: a – image of SE plate surface; b – image of BSE plate surface; c – results of chemical analysis at point 1; g – results of chemical analysis at point 2; d – results of chemical analysis at point 3.

Table 3 presents the results of the study of the alloy impurity composition.

Table 3. Impurity composition of the alloy.

Alloy	Oxygen, mass %	Nitrogen, mass %	Hydrogen, mass %	Carbon, mass %	Sulfur, mass %
Ti-38Zr-11Nb	0,02 ± 0,005	0,0059 ± 0,004	0,0064 ± 0,001	0,017 ± 0,005	0,0054 ± 0,0009

The results of chemical analysis showed that the obtained alloys correspond to GOST 19807-91 [10] for titanium alloys of the VT1-0 type in terms of the amount of impurities.

3.2. Optical Microscopy of Microstructures of Ti-38Zr-11Nb Plates

Figure 3 shows the microstructures of the plates after quenching, obtained by studying the cross-section relative to the rolling direction.

 doi:10.20944/preprints202502.1884.v1

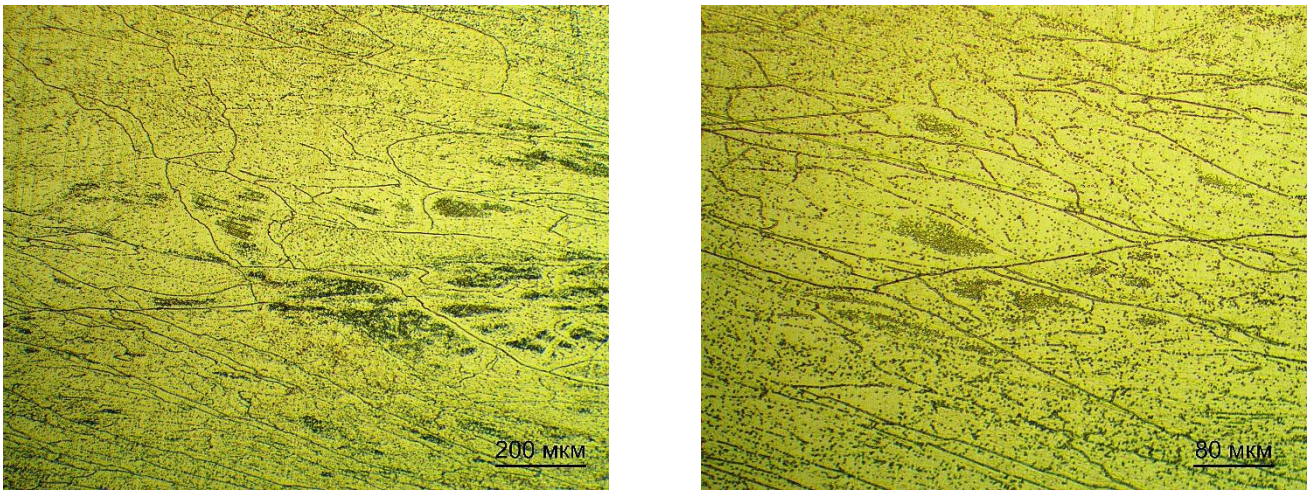

(a) (b)

Figure 3. Microstructure of Ti-38Zr-11Nb alloy plates after quenching.

Figure 4 shows the microstructures of the plates after quenching and annealing at 400°C for 1 hour in vacuum, obtained by examining the cross section relative to the rolling direction.

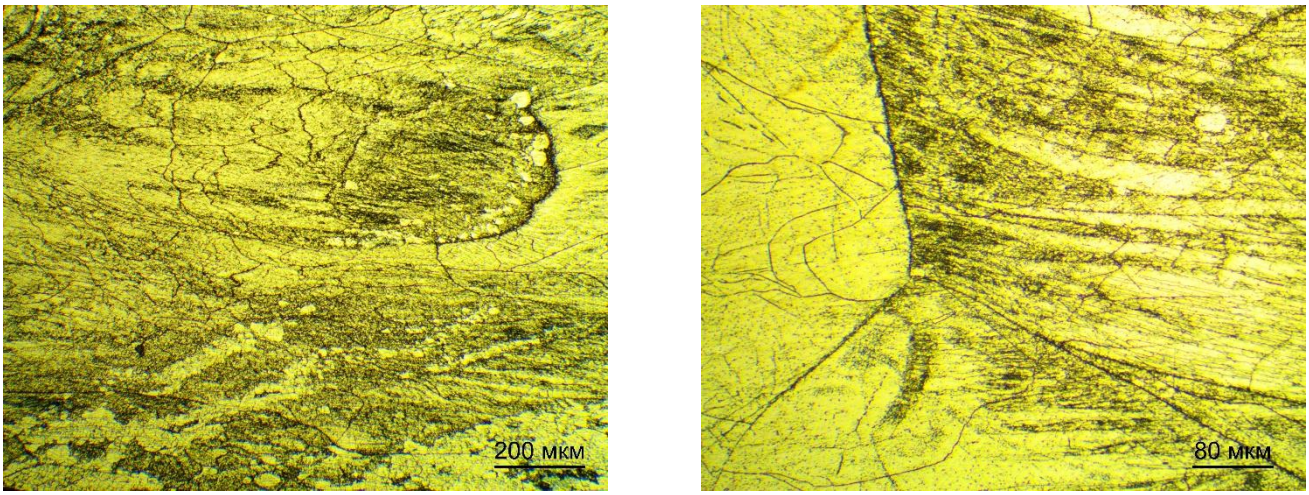

(a) (b)

Figure 4. Microstructure of Ti-38Zr-11Nb alloy plates after quenching and annealing.

After quenching, the microstructure of the plates in the longitudinal and transverse sections is not uniform and consists of β-grains of elongated shape along the rolling direction. The non-uniformity of the grains can be explained by insufficient preheating of the blanks before contact with the massive cold rolls of the rolling mill, while the quenching time is insufficient for recrystallization. Annealing allows the recrystallization process to occur at a low temperature due to sufficient exposure time and possible excess internal energy in the grains after quenching. Grain growth is associated with the recrystallization process, and the formation of subgrains is observed at the same time.

3.3. X-Ray Phase Analysis (XRF) of Ti-38Zr-11Nb Alloys

The results of X-ray phase analysis of the plates after rolling with quenching and rolling with quenching and annealing are presented in Table 4. The alloys after quenching and quenching with annealing consist only of β-Ti. This is due to the influence of the β-stabilizer Nb and the neutral element Zr. Zirconium alone is a neutral hardener, but in the presence of other β-stabilizers, it also weakly stabilizes the β-phase. [11] The phase composition does not change after annealing. This

 doi:10.20944/preprints202502.1884.v1

confirms that long-term use of the studied material after quenching during aging will not change its phase, and accordingly, Young's modulus will not increase to high values.

From the diffraction patterns in Figure 5 it is evident that the sample of the material with the studied amount of Nb, the formation of α'-Ti and ω-Ti after quenching is suppressed and completely replaced by β-Ti.

Table 4. Phase composition of Ti-38Zr-11Nb alloy plates.

Composition	Condition	Phase Structure	Type of Crystal Lattice	Contents, Volume. %	Crystal Lattice Parameters
Ti-38Zr-11Nb	After the rolling process and quenching	β-Ti	type A2, cI2	100	a = 3.4 ± 0.01 Å
	After the rolling process, quenching and annealing	β-Ti	type A2, cI2	100	a = 3.4 ± 0.01Å

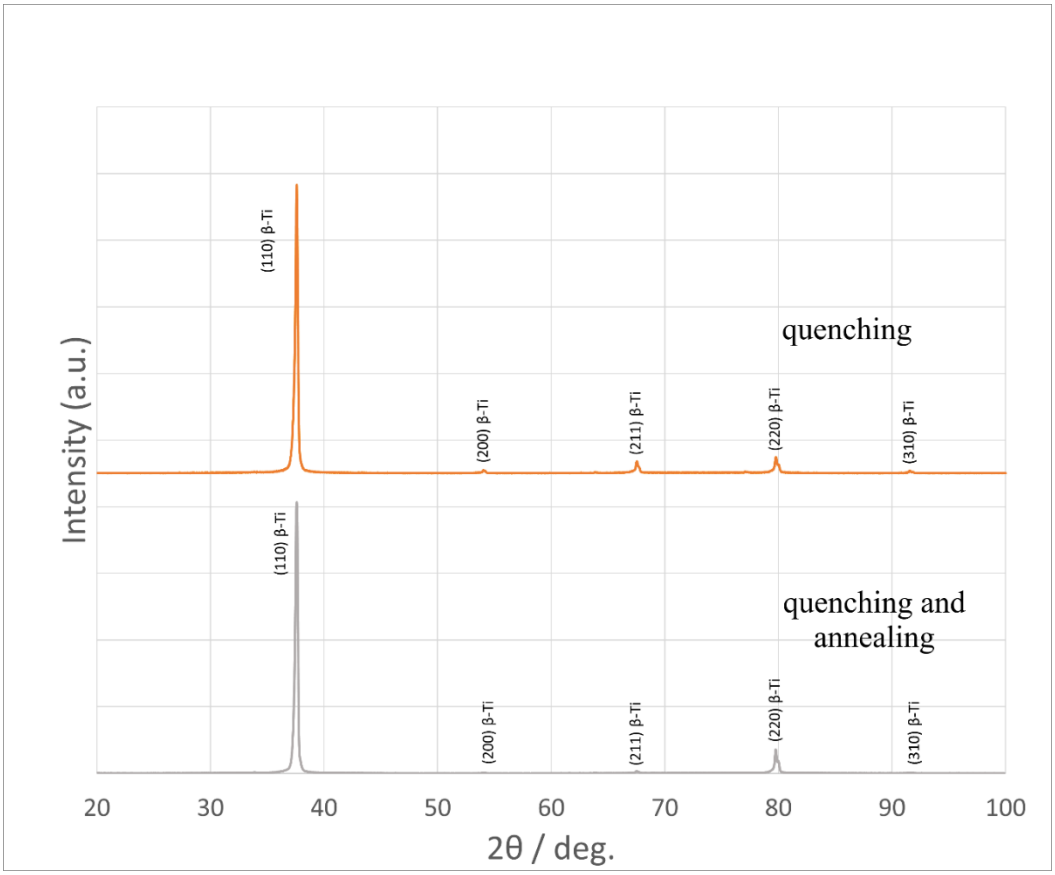

Figure 1. X-ray diffraction patterns of alloys.

3.4. Nanohardness of Ti-38Zr-11Nb Alloy

The nanohardness of Ti-38Zr-11Nb alloy samples in the condition after quenching from 600°C, as well as after quenching from 600°C and annealing at 400°C for 1 hour was determined using the nanoindentation method. The results are presented in Figure 16 and Table 5.

Table 5. Nanohardness of Ti-38Zr-11Nb plates.

Composition	Condition	Nanohardness, HV
Ti-38Zr-11Nb	After the rolling process and quenching	258 ± 7

 doi:10.20944/preprints202502.1884.v1

	After the rolling process, quenching and annealing	236 ± 10

The nanohardness of the plates decreases slightly after annealing, which is associated with an increase in grain size due to partial recrystallization and a decrease in dislocation density, while the phase composition remains the same. Unlike microhardness, which reflects average properties at the microstructure level, nanohardness is measured at ultra-low loads (millinewtons) and allows the analysis of local mechanical properties at the level of individual grains, their boundaries or nanoscale regions. This makes the nanohardness method highly sensitive to microstructural changes such as recrystallization, subgrain formation, redistribution of residual stresses or the appearance of nanoclusters that are not detected by X-ray diffraction. However, due to the local inhomogeneity of the material, the correct interpretation of the data requires an increase in the number of measurements per sample to ensure the statistical reliability of the results when analyzing subtle effects, including the evolution of the defect structure.

3.5. Mechanical Properties

Mechanical test results for the Ti-38Zr-11Nb alloy are shown in 6. Typical tensile diagrams are shown in Figure 2.

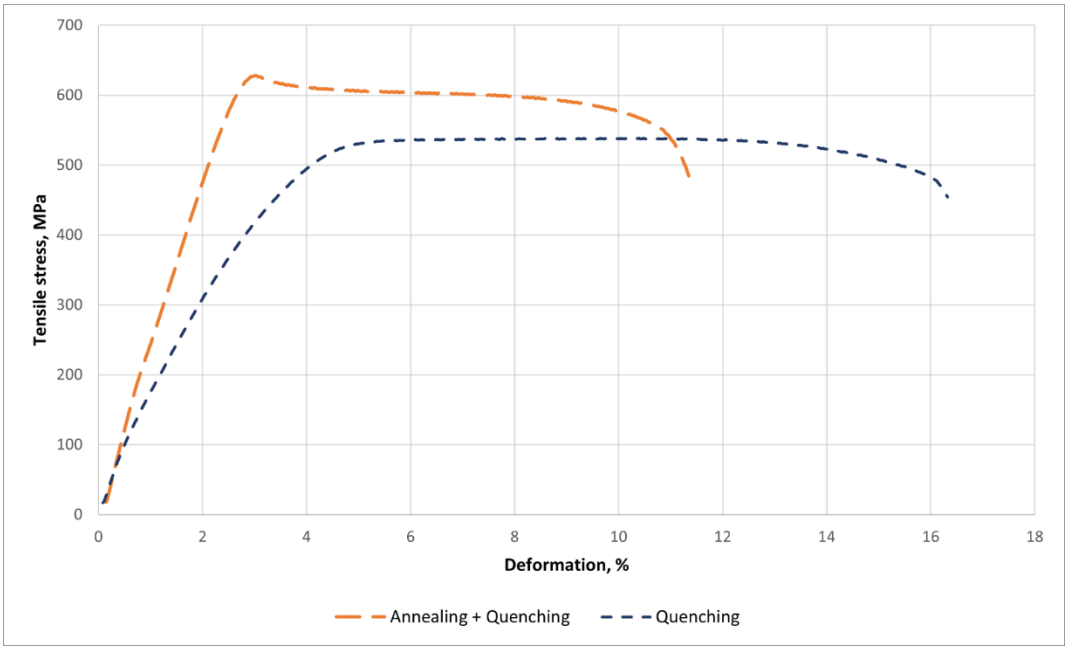

Figure 2. Tensile diagram of Ti-38Zr-11Nb alloy samples.

Table 6. Mechanical properties of Ti-38Zr-11Nb plates.

State	δ, %	σ0.2, MPa	σв, MPa
Ti-38Zr-11Nb			
After the rolling process and quenching	12.2± 1.4	371± 35	529± 14
After the rolling process, quenching and annealing	9.3 ± 0.7	614 ± 20	628 ± 14

The yield strength has almost doubled, from 371 to 614 MPa. The tensile strength has also increased, but not as significantly, from 529 to 628 MPa. The relative elongation has decreased by 32%, indicating a decrease in ductility. Based on the XRD data on the preservation of the cubic beta phase and microstructural changes such as grain size, it can be assumed that the presence of

 doi:10.20944/preprints202502.1884.v1

subgrains leads to an increase in strength and a decrease in ductility. Residual stresses or defect distribution may also play a role. After quenching, the material may have a high dislocation density and residual stresses. Low-temperature annealing can promote the relaxation of these stresses and the redistribution of dislocations, possibly forming a more stable structure, for example, the transition from an unstable beta phase to a stable one. This can increase the yield strength and strength due to dislocation hardening, but reduce ductility due to a decrease in the ability to deform. It is also possible that annealing has caused the atoms in the beta phase to become ordered, creating a short-range order that is not detectable by X-ray diffraction but affects the mechanical properties. The ordered structure can impede the movement of dislocations, increasing strength but making the material more brittle.[XXX] Another factor is the change in grain size and the formation of subgrains observed in optical studies - the formation of a submicrostructure has occurred, which increases strength. It is also worth considering the possible release of very small amounts of other phases that are not detected by X-ray diffraction due to their small size or low concentration. For example, nanoscale clusters or phase nuclei that do not form a crystal lattice distinguishable by X-ray diffraction.

3.6. Cyclical Loading

Figure 3 shows the tensile diagrams for cyclic loading up to 8% strain for 10 cycles.
This alloy does not have superelasticity.

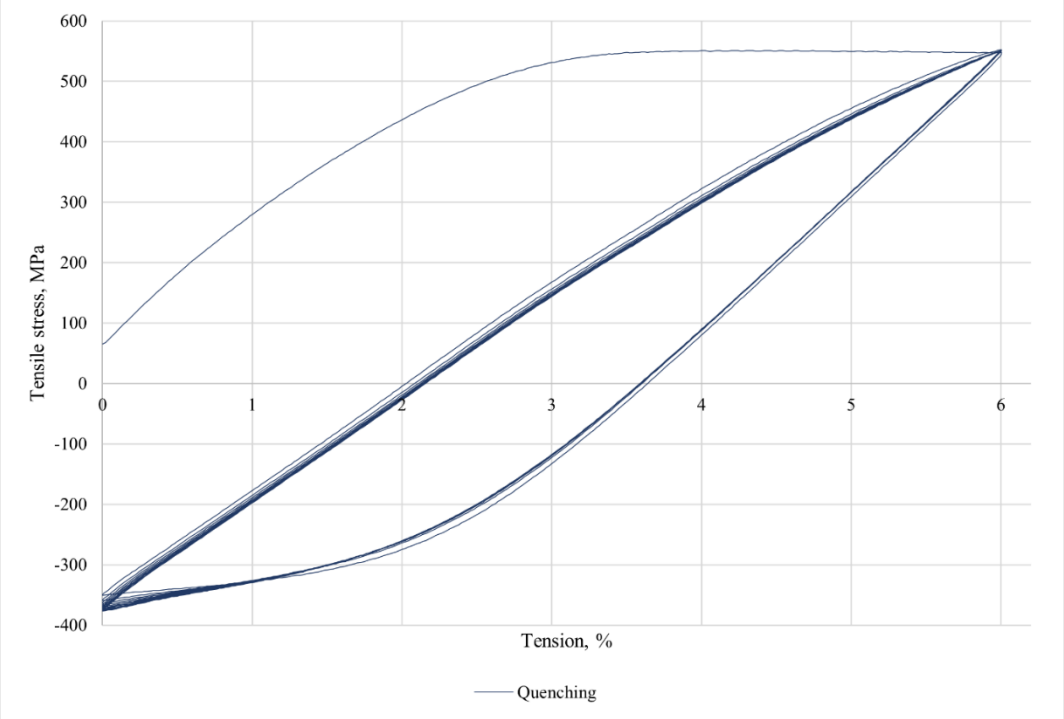

Figure 3. Cyclic loading of the alloy Ti-38Zr-11Nb.

3.7. Young's Modulus

The Young's modulus of the alloys after quenching from 600°C and annealing at 400°C for 1 hour was determined using the nanoindentation method.

An example of a loading diagram during indentation is shown in Figure 8. The results of the study of the elastic modulus of plates after rolling and quenching are presented in Table 7.

 doi:10.20944/preprints202502.1884.v1

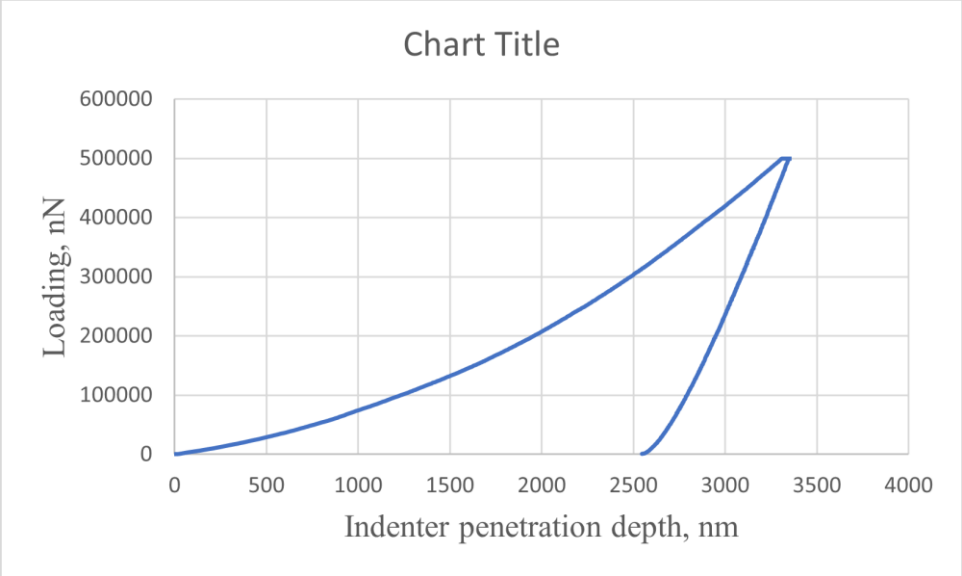

Figure 4. Typical diagram of alloy loading during indentation into the alloy after annealing.

Table 7. Young's modulus values of plates.

Composition	E, GPa
After the rolling process and quenching	85 ± 3
After the rolling process, quenching and annealing	81 ± 2

The decrease in Young's modulus from 85 GPa to 81 GPa after low-temperature annealing, with preservation of the β-phase, may be due to microstructural changes: Relaxation of residual stresses from quenching reduces distortions in the crystal lattice, reducing its local stiffness; atomic ordering (short-distance order) or redistribution of alloying elements in the β-matrix alters interatomic interactions, affecting the elastic properties; a decrease in dislocation density during annealing weakens their contribution to elastic strength; and the possible formation of nano-sized clusters or local inhomogeneities, not detected by X-ray diffraction, modifies the deformation response. These processes, without affecting the phase composition, reduce the global stiffness of the material, which is manifested by a decrease in Young's modulus during nanoindentation.

3.8. Fractography

Figure 8 shows a typical view of the fracture surface under static loading for samples of Ti-38Zr-11Nb alloy after rolling and quenching: 1—ductile fracture zone with noticeable material flow; 2—ductile fracture zone with formation of a microporous surface; 3—brittle fracture zone; 4—location of fracture onset.

 doi:10.20944/preprints202502.1884.v1

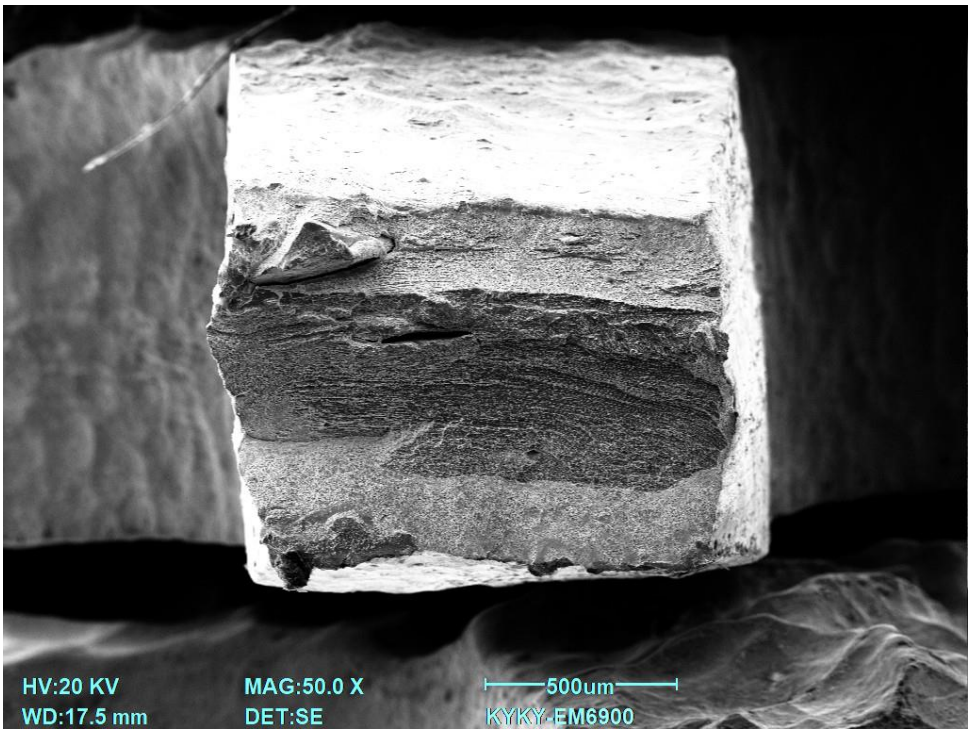

(a)

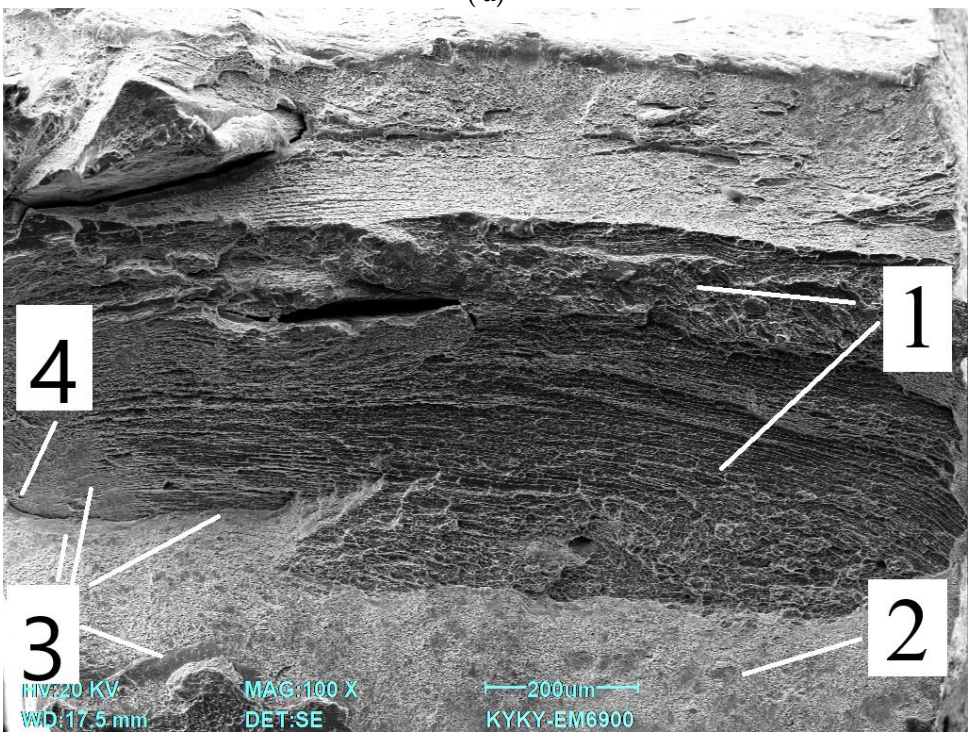

(b)

 doi:10.20944/preprints202502.1884.v1

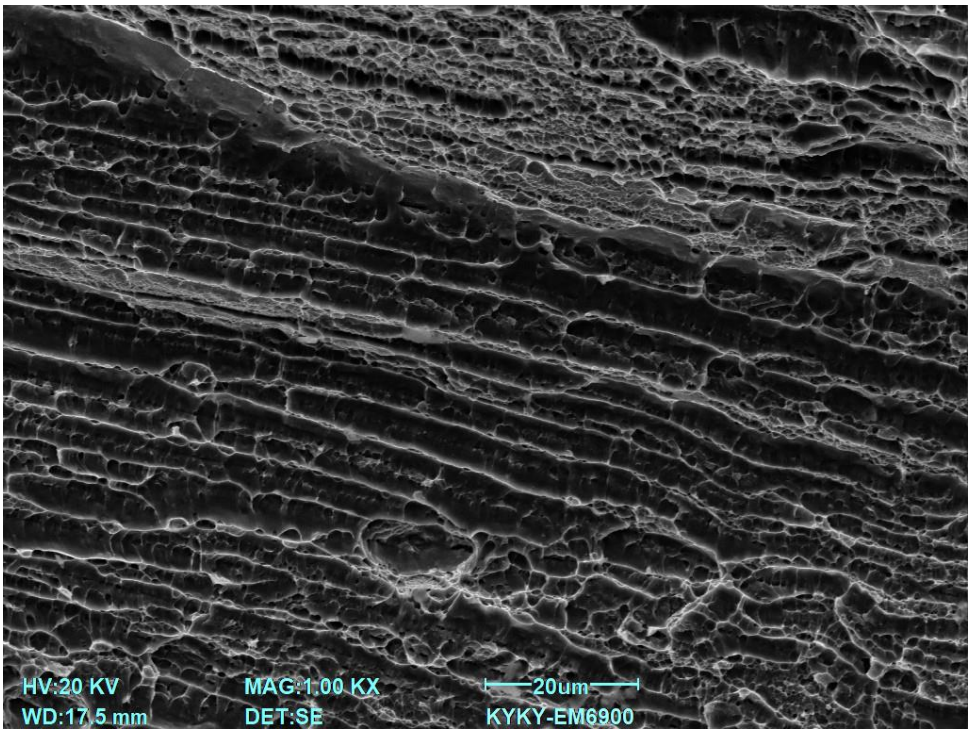

(c)

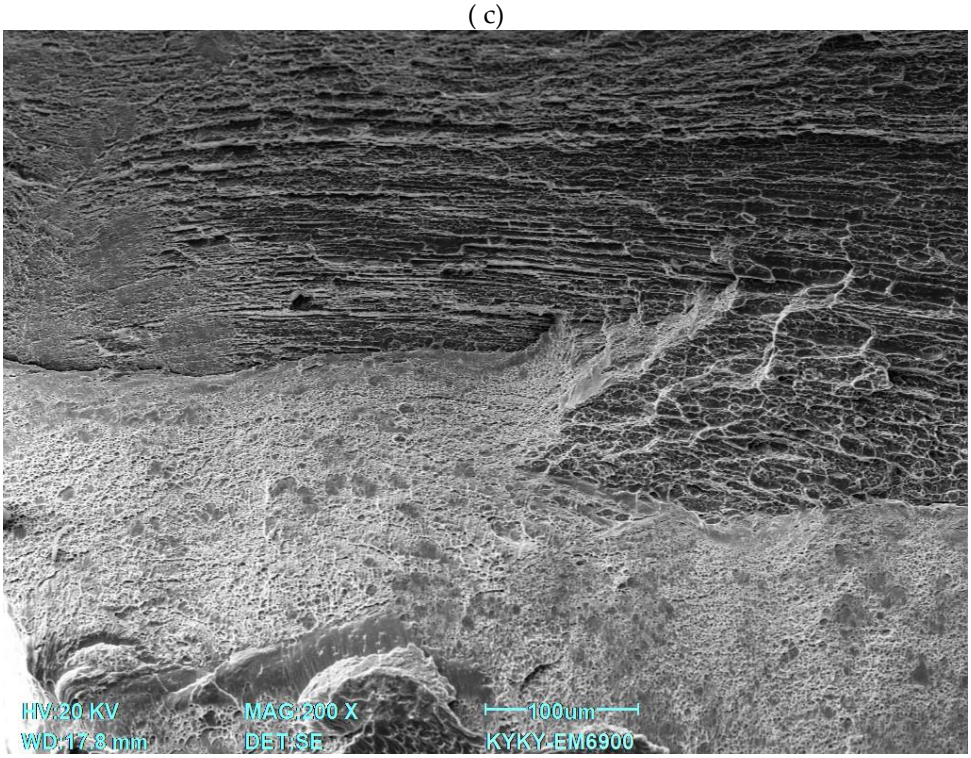

(d)

Figure 9. Fractography of Ti-40Zr-9Nb alloy after rolling and quenching: (a) General view; (b) Fracture surface; (c) Central part; (d) Zone with the presence of brittle fracture.

SEM images show typical signs of tensile failure of beta titanium alloy. Visual analysis reveals the following key features: large areas with tensile structures are visible; areas of microporosity are present, which may be the result of the formation of plastic flow cells prior to fracture, characteristic of plastic failure; areas with smooth surfaces are noticeable, which may indicate brittle local failure. At the same time, it is possible to note the presence of a layered structure, i.e., a central, more viscous area and an area of increased plastic deformation on the outside, which was created during the production of the specimens, in which a high degree of deformation accumulates precisely on the

 doi:10.20944/preprints202502.1884.v1

sides of the specimen in contact with the rolls of the rolling mill. On a large scale, it can be seen that the pits are not uniform in size, and some of them are connected by narrow bridges. This confirms the active plastic flow of the material. Small intercellular cracks are present, which may indicate localized zones of brittle failure under peak loads.

4. Conclusions

The beta phase in the Ti-38Zr-11Nb alloy was detected as expected after quenching and confirmed after low-temperature annealing. This confirms the long-term stability of the phase composition, which is important for the use of the material in implantology.

The uniform distribution of elements (Ti, Zr, Nb) in the alloy contributes to the homogeneity of its mechanical properties and biocompatibility, and the presence of zirconium in combination with niobium stabilizes the beta phase, improving the mechanical properties.

The low modulus of elasticity (reduction from 85 GPa to 81 GPa after annealing) brings the mechanical properties of the alloy closer to those of bone tissue, minimizing the risk of stress shielding and improving the biomechanical compatibility of the implant. The increase in strength properties (yield strength increased from 371 to 614 MPa) after quenching and annealing is associated with recrystallization, subgrain formation, redistribution of residual stresses and dislocation strengthening. These changes result in improved mechanical stability of the implant.

The plasticity of the material decreased (relative strain decreased by 32%) due to the formation of an ordered structure that prevents dislocation movement and local microstructural changes.

Microstructural analysis revealed that the material shows signs of plastic failure with local zones of brittle failure, which requires further optimization of composition and processing to increase durability and reliability.

The absence of α' and ω phase formation (within the sensitivity of the device) after heat treatment confirms the stabilizing effect of niobium and zirconium on the beta phase, which is important for maintaining a low elastic modulus and biocompatibility of the material.

Analytical methods (energy dispersive spectrometry, X-ray phase analysis, nanohardness) confirmed the high homogeneity and stability of the material properties, making the Ti-38Zr-11Nb alloy a promising candidate for use in hip arthroplasty.

Author Contributions: Conceptualization, S.V.K. and L.A.S.; Data curation, M.A.K., E.O.N. and L.A.S.; Formal analysis, K.V.S. and S.V.K.; Funding acquisition, M.A.S. (Mikhail A. Sevostyanov); Investigation, A.P.C., A.V.S., B.A.R., T.M.S. and S.A.M.; Methodology, I.V.B., A.V.S., M.A.S. (Maria A. Sudarchikova), M.E.P., E.E.B., T.M.S. and S.A.M.; Project administration, M.A.S. (Mikhail A. Sevostyanov) and A.G.K.; Resources, E.O.N. and A.G.K.; Supervision, M.L.K., A.D.G.; Validation, A.D.G., B.A.R., Y.A.M., M.E.P.; Visualization, E.E.B., A.P.C., M.L.K., I.V.B. and Y.A.M.; Writing—original draft, K.V.S.; Writing—review and editing, M.A.K. and M.A.S. (Maria A. Sudarchikova) All authors have read and agreed to the published version of the manuscript.

Funding: This work was supported by the grant of the Russian Science Foundation No. 24-13-00186, https://rscf.ru/project/24-13-00186/.

Institutional Review Board Statement: Not applicable.

Data Availability Statement: The original contributions presented in this study are included in the article/supplementary material. Further inquiries can be directed to the corresponding author(s).

Conflicts of Interest: The authors declare no conflicts of interest. The funders had no role in the design of the study; in the collection, analyses, or interpretation of data; in the writing of the manuscript; or in the decision to publish the results. All the authors have reviewed the manuscript and agree on submission to your journal.

References

1. Galmiche R, Migaud H, Beaulé PE. Hip Anatomy and Biomechanics Relevant to Hip Replacement // Personalized Hip and Knee Joint Replacement [Internet], **2020**, Vol. 2, DOI: 10.1007/978-3-030-24243-5_2.

2. Shichman I, Roof M, Askew N, Nherera L, Rozell JC, Seyler TM, Schwarzkopf R. Projections and Epidemiology of Primary Hip and Knee Arthroplasty in Medicare Patients to 2040-2060 // JB JS Open Access, **2023**, Vol. 8(1):e22, DOI: 10.2106/JBJS.OA.22.00112.
3. Maradit Kremers H, Larson DR, Crowson CS, Kremers WK, Washington RE, Steiner CA, Jiranek WA, Berry DJ. Prevalence of Total Hip and Knee Replacement in the United States // J Bone Joint Surg Am., **2015**, Vol. 97(17):1386-97, DOI: 10.2106/JBJS.N.01141.
4. Chang Yong Hu, Taek-Rim Yoon. Recent updates for biomaterials used in total hip arthroplasty // Biomater Res, **2018**, Vol. 22:33, DOI: 10.1186/s40824-018-0144-8.
5. Sathishkumar S., Paulraj Jawahar, Chakraborti Prasun, Muthuraj Muthusivaramapandian. Comprehensive Review on Biomaterials and Their Inherent Behaviors for Hip Repair Applications // ACS Applied Bio Materials, **2023**, Vol. 6, No. 11. pp. 4439-4464, DOI: 10.1021/acsabm.3c00327.
6. Merola M, Affatato S. Materials for Hip Prostheses: A Review of Wear and Loading Considerations // Materials (Basel), **2019**, Vol. 12(3):495, DOI: 10.3390/ma12030495.
7. Allergic Reaction to Vanadium Causes a Diffuse Eczematous Eruption and Titanium Alloy Orthopedic Implant Failure // Contact Dermatitis, **2017**, Vol. 99(4). pp. 245-249.
8. Zhong Q, Pan X, Chen Y, Lian Q, Gao J, Xu Y, Wang J, Shi Z, Cheng H. Prosthetic Metals: Release, Metabolism and Toxicity // International Journal of Nanomedicine , **2024**, Vol. 2024:19. P. 5245—5267, DOI: 10.2147/IJN.S459255.
9. T. R. The toxicity of metals used in orthopaedic prostheses. An experimental study using cultured human synovial fibroblasts // J Bone Joint Surg Br., **1981**, Vol. 63-B(3), No. 435-40, DOI: 10.1302/0301-620X.63B3.7263760.
10. N. E. Corrosion of Metallic Biomaterials: A Review // Materials (Basel), **2019**, Vol. 12(3):E407, DOI: 10.3390/ma12030407.
11. Morgan E.F., Unnikrisnan G.U., Hussein A.I. Bone Mechanical Properties in Healthy and Diseased States // Annu Rev Biomed Eng., **2018**, Vol. 20. pp. 119-143, DOI: 10.1146/annurev-bioeng-062117-121139.
12. Krisztián Kovács, Szilárd Váncsa, Gergely Agócs, Andrea Harnos, Péter Hegyi, Viktor Weninger, Katinka Baross, Bence Kovács, Gergely Soós, György Kocsis, Anisotropy. Anisotropy, Anatomical Region, and Additional Variables Influence Young's Modulus of Bone: A Systematic Review and Meta-Analysis // JBMR Plus, **2023**, Vol. 7, No. 12. P. e10835, DOI: 10.1002/jbm4.10835.
13. 13.
14. M. Amirhosseini. Aseptic Loosening of Orthopedic Implants : Osteoclastogenesis Regulation and Potential Therapeutics. **2019**.
15. Keller, T. S., Mao, Z., & Spengler, D. M.. Young's modulus, bending strength, and tissue physical properties of human compact bone // Journal of orthopaedic research : official publication of the Orthopaedic Research Society, **1990**, Vol. 8, No. 4. pp. 592–603, DOI: 10.1002/jor.1100080416.
16. Hoffmeister, B. K., Smith, S. R., Handley, S. M., & Rho, J. Y.. Anisotropy of Young's modulus of human tibial cortical bone // Medical & biological engineering & computing, **2000**, Vol. 38, No. 3. pp. 333–338, DOI: 10.1007/BF02347055.
17. Raffa, M.L.; Nguyen, V.-H.; Hernigou, P.; Flouzat-Lachaniette, C.-H.; Haiat, G.; Traumatologique, H.; Mondor, A.-H.; Paris, C.. Stress shielding at the bone-implant interface: Influence of surface roughness and of the bone-implant. // J. Orthop. Res., **2021**, Vol. 39. pp. 1174–1183, DOI: 10.1002/jor.24840.
18. Noyama, Y.; Miura, T.; Ishimoto, T.; Itaya, T.; Niinomi, M.; Nakano, T. Bone loss and reduced bone quality of the human femur after total hip arthroplasty under stress-shielding effects by titanium-based implant. // Materials Transactions, **2012**, Vol. 53. pp. 565–570, DOI: 10.2320/matertrans.M2011358.
19. Shahzamanian, M.; Banerjee, R.; Dahotre, N.B.; Srinivasa, A.R.; Reddy, J. Analysis of stress shielding reduction in bone frac-ture fixation implant using functionally graded materials // composition structure, **2023**, Vol. 321, DOI: 10.1016/j.compstruct.2023.117262.
20. Zhang Q. H., Cossey A., Tong, J. tress shielding in periprosthetic bone following a total knee replacement: Effects of implant material, design and alignment // Medical engineering & physics, **2016**. pp. 1481–1488, DOI: 10.1016/j.medengphy.2016.09.018.

 doi:10.20944/preprints202502.1884.v1

21. D. Vogel, M. Klimek, M. Saemann, R. Bader. Influence of the Acetabular Cup Material on the Shell Deformation and Strain Distribution in the Adjacent Bone—A Finite Element Analysis // Materials, **2020**, Vol. 13, DOI: 10.3390/ma13061372.
22. Anca Fratila, Cristina Jimenez-Marcos, Julia Claudia Mirza-Rosca, Adriana Saceleanu. Mechanical properties and biocompatibility of various cobalt chromium dental alloys // Materials Chemistry and Physics, **2023**, DOI: 10.1016/j.matchemphys.2023.127867.
23. Aherwar Amit, Singh A.K., Patniak Amar. Cobalt based alloy: A better choice biomaterial for hip implants // Trends in Biomaterials and Artificial Organs, **2016**, Vol. 30.
24. Fedorenko Alexey, Fedulov Boris, Evlashi Stanislav,Staroverov Oleg, Pankov Alexander, Shalnova Svetlana, Lomakin Evgeny. Experimental studies and the model of anisotropic plasticity for additively manufactured stainless steel with stress state dependent properties // Continuum Mechanics and Thermodynamics, **2024**, Vol. 36, No. 3. pp. 619-637, DOI: 10.1007/s00161-024-01286-4.
25. Birgit Rehmer, Faruk Bayram, Luis Alexander Ávila Calderón, Gunther Mohr, Birgit Skrotzki. Elastic modulus data for additively and conventionally manufactured variants of Ti-6Al-4V, IN718 and AISI 316 L // Scientific Data (Nature), **2023**, Vol. 10, No. 474, DOI: 10.1038/s41597-023-02387-6.
26. Volchikhina M., Konushkin S., Mikhlik S., Sergienko K., Kaplan M., Gorbenko A., Sevostyanova T., Kolmakov, A., Sevostyanov, M. The Structure and Mechanical Properties of Ti–(36–40)Zr–9Ta (at %) Alloys for Medical Purposes // Inorganic Materials: Applied Research, **2024**, Vol. 15. pp. 1321-1328, DOI: 10.1134/S2075113324700941.
27. Hussein, M.A.; Mohammed, A.S.; Al-Aqeeli, N. Wear Characteristics of Metallic Biomaterials: A Review // Materials, **2015**, Vol. 8. pp. 2749-2768, DOI: 10.3390/ma8052749.
28. Leite Karla, Dia Millene, Tavares, Fernanda, Chevitarese Ana, Martins Mariana, Masterson Danielle, Menezes Livia, Gonçalves Andréa, Maia Lucianne. A Data Mining Analysis on Niobium in Dentistry: Promising Alloys for Dental Materials // Pesquisa Brasileira em Odontopediatria e Clínica Integrada, **2024**, Vol. 24, DOI: 10.1590/pboci.2024.092.
29. Hsu H.C.; Wu S.C.; Fang W.C.; Ho W.F. Experimental Investigation of the Impact of Niobium Additions on the Structural Characteristics and Properties of Ti–5Cr–xNb Alloys for Biomedical Applications // Materials, **2024**, Vol. 17. P. 1667.
30. Marković G.; Manojlović V.; Ružić J.; Sokić M. Predicting Low-Modulus Biocompatible Titanium Alloys Using Machine Learning // Materials, **2023**, Vol. 16. P. 6355.
31. Tang J.; Yang H.; Qian B.; Zheng Y.; Vermaut P.; Prima F.; Sun F. TWIP-assisted Zr alloys for medical applications: De-sign strategy, mechanical properties and first biocompatibility assessment // Journal of Materials Science and Technology , **2024**, Vol. 184. pp. 32-42.
32. Chattopadhyay K.; Mandal M.; Maiti D.K. A review on zirconium-based metal–organic frameworks: Synthetic approaches and biomedical applications // Materials Advances, **2024**, Vol. 5. pp. 51-67.
33. Weiss I., Semiatin S.L. Thermomechanical processing of beta titanium // Materials Science and Engineering, **1998**, Vol. A243. pp. 46-65, DOI: 10.1016/s0921-5093(97)00783-1.
34. Wang, Q., Dong, C. & Liaw, P.K. Structural Stabilities of β-Ti Alloys Studied Using a New Mo Equivalent Derived from [β/(α + β)] Phase-Boundary Slopes // Metall Mater Trans A , **2015**, Vol. 46. pp. 3440-3447, DOI: 10.1007/s11661-015-2923-3.
35. Sergienko, K. V., Konushkin, S. V., Kaplan, M. A., Gorbenko, A. D., Guo, Y., Nasakina, E. O., Sudarchikova, M. A., Sevostyanova, T. M., Morozova, Y. A., Shatova, L. A., Mikhlik, S. A., Sevostyanov, M. A., & Kolmakov, A. G.. Physical and Mechanical Properties of Ti-Zr-Nb Alloys for Medical Use // Metals, **2024**, Vol. 14, No. 1311, DOI: 10.3390/met14111311.
36. ISO 14577-1:2002. Metallic materials — Instrumented indentation test for hardness and materials parameters, Geneva, Switzerland, **2002**.
37. GOST 19807-91, High-alloyed corrosion-resistant and heat-resistant steels and alloys. Grades, Russian State Standard // (in Russian), **1991**.
38. Elias L.M., Schneider S.G., Knopf-Marques Helena, Malvisi F. Microstructure and mechanical characterization of biomedical Ti–Nb–Zr // Materials Science and Engineering: A, **2006**, Vol. 432. pp. 108-112, DOI: 10.1016/j.msea.2006.06.013.

 doi:10.20944/preprints202502.1884.v1